Syneresis of self-crowded calcium-alginate hydrogels as a self-driven athermal aging process

Bruno da Silva Pinto, Olivier Ronsin, Tristan Baumberger

Syneresis of self-crowded calcium-alginate hydrogels as a self-driven athermal aging process

Bruno Da Silva Pinto, Olivier Ronsin, and Tristan Baumberger

Sorbonne Universités, CNRS, Institut des nanosciences de Paris 4, place Jussieu, F-75005 Paris and Université Paris Cité, F-75006 Paris

(Dated: November 29, 2022)

Abstract

The assembly of biopolymers into a hydrated elastic network often goes along with *syneresis*, a spontaneous process during which the hydrogel slowly shrinks and releases solvent. The tendency to syneresis of calcium-alginate hydrogels, widely used biocompatible materials, is a hindrance to applications for which dimensional integrity is crucial. Although calcium-induced aggregation of specific block-sequences has been long known as the microscopic process at work in both primary cross-linking and syneresis, the nature of the coupling between these structural events and the global deswelling flow has remained so far elusive. We have tackled this issue within the regime of entangled pregels that yield highly cross-linked, self-crowded hydrogels with stiff networks. Using an original, stopped-flow extrusion experiment, we have unveiled a robust, stretched-exponential kinetics of shrinking, spanning more than six decades of time and quasi-independent of the alginate concentration. A careful analysis of the puzzling dynamical features of syneresis in these gels has led us to propose that due to the network rigidity, the calcium-fueled, random collapse events that drive solvent locally, are not thermally activated but rather controlled by the average poroelastic flow itself, according to a self-sustained mechanism described here for the first time.

I. INTRODUCTION

Alginate gels are the archetype of ionotropic hydrogels, the setting and degradation of which can be controlled by the nature and amount of ions present in their aqueous solvent. In parallel with their long-standing applications in the food industry e.g. as low-fat substitutes, owing to their bio-degradability, bio-compatibility and non-immunogenicity, they find utility in numerous biomedical applications such as wound dressings, drug- or cell-delivery carriers, scaffolds for tissue engineering or model extracellular matrix for *in vitro* cell experiments[1].

Correlatively, the mechanism of ionic gelation of alginate has motivated a large amount of studies since the pioneering work of Rees *et al*[2] who coined the successful phrase "egg-box model" to describe the cross-link zone involving an alginate dimer and binding divalent cations, such as Ca^{2+} (Fig.1). Alginates in their salt form are negatively charged polysaccharides extracted from seaweeds[3]. They are linear copolymers of mannuronate (M) and guluronate (G) residues arranged in a blockwise pattern interspersed with alternating (MG...) sequences. Due to its steric and electric charge arrangement, a G-block dimer ("box") can chelate ions ("eggs") and form an extended cross-link zone stabilized by electrostatic interactions[4]. The kinetics of building a three-dimensional network (gelation) via ionic cross-linking has been actively studied, both experimentally and theoretically[5–7]. Egg-box assembly is found to be a fast process limited by the supply of ions. In many applications, including 3D-printing[8, 9], sodium alginate pregel is poured as a spherical drop or a cylindrical fiber[10, 11] in a bath containing the binding ions which must diffuse from the surface inwards in order to form cross-links ("external gelation").

When ions are provided in excess with respect to the stoechiometry of G-block dimerisation, alginate gels slowly shrink[12, 13]. The associated solvent release is known as "syneresis" in the food industry. It represents a major challenge in the manufacturing of food gels: whereas draining water out of the gel matrix is a constitutive step for cheese processing, keeping it in is preferable for yoghurts or jellies[14]. When biopolymer (e.g. agarose) gel plates are used as cell-culture medium, syneresis may generate strong internal stresses and ultimately lead to the unwanted detachment of the plates from the walls of Petri dishes [15].

Generally speaking, syneresis can be seen as an indication that gelation is an ongoing network/solvent phase separation, slowed down and eventually arrested by elastic and topological constraints. As such the extend and kinetics of deswelling must be expected to

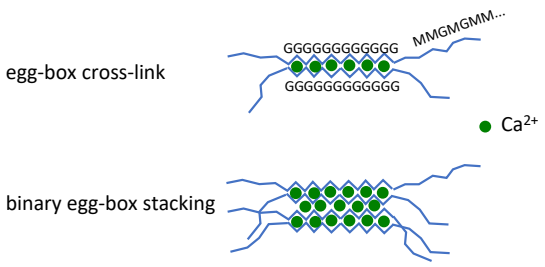

FIG. 1. Schematic representation of the two aggregation mechanisms invoked in this study. Alginate chains are composed of sequences of Mannuronate (M) and Guluronate (G) units (residues). An "egg-box" cross-link of functionality 4 involves the binding by Ca^{2+} ions of two "G-blocks" composed of contiguous G units. Sequences involving MM or alternating MG units do not form stable calcium-bound structures. Higher order calcium-induced G-block aggregation is possible. For instance, two egg-boxes can stack to form a cross-link of functionality 8.

depend strongly on the nature of the cross-linking process. In the case of alginate gels[3], the correlation between syneresis and an excess of binding ions points towards multimer, ion-induced aggregation of G-blocks (Fig.1), as the motor for network shrinking[12, 16]. This picture was confirmed by small angle X-ray scattering[13].

From a practical point of view, syneresis is hindered by limiting the amount[12] or the activity (concentration)[17] of available binding ions. Interestingly, *flexibility* of the network strands has been clearly identified as a factor favoring syneresis[13] from diluted pregels. It can be controlled to some extent by the cross-link density, the molar mass and the residue arrangement of the alginate chains. However, since native alginate chains are only semi-flexible, a property they share with many biopolymers[18], large flexibility was only achieved thanks to a smart biochemical tool, namely C5-epimerase, an enzyme able to change the block structure of a chain into a strictly alternating MGMG... flexible sequence[19][13].

Beyond these useful rules of thumb, the basic physico-chemical mechanisms of syneresis in alginate gels remain elusive. In particular, there is no prediction of the stœchiometry of the G-block association driving syneresis, the value of the equilibrium volume ratio (even the existence of such an equilibrium) the nature of the aggregation/deswelling coupling and, above all, the kinetics of syneresis. This is all the more surprising as alginate can be considered as a model system for associating biopolymer gels owing to the advanced

structural knowledge gained over half a century of research.

In the present study we have focused on a single, G-rich sodium alginate and, at odds with previous reports, we have worked with *concentrated* pregel solutions, i.e. well above the entanglement concentration, where chain mobility and flexibility are strongly reduced. Using an original stopped-flow experiment we have characterized the kinetics of deswelling of extruded gel fibres over unprecedented long times. Quite unexpectedly inasmuch as the self-crowded regime is hardly amenable to a straightforward polymer physics model, we unveiled a kinetic behavior quasi-independent of the alginate concentration, which boiled down to a few robust features: (i) The primary gelation stage during which the cylindrical sample retains its dimensions is clearly separated from the syneresis one proper; (ii) The latter is a very slow process. It exhibits a long-tailed kinetics; (iii) It eventually reaches an apparent saturation at a deswelling volumetric ratio close to 0.5; (iv) The whole relaxation time spectrum scales diffusively with the square of the fibre radius.

We study the primary gelation kinetics (section III A) using a model compatible with the low alginate mobility in the self-crowded pregel. We deduce the amount of calcium ions chelated in egg-boxes from which we estimate the average distance between cross-links. Comparison with the persistence length of alginate chains leads to anticipate a strong filamentous *rigidity* of the alginate network. Following this guideline we analyse (section IV) the kinetics of syneresis and construct a scenario accounting for the most unexpected experimental features: the existence of a "magic" 1/2 deswelling ratio at saturation and the *global* diffusive scaling of the transient kinetics, including the stretched-exponential tail usually ascribed to slow *local* rearrangements. We propose (section IV A) that syneretic deswelling results from the free-volume loss associated with the calcium-induced, binary stacking of neighbouring egg-boxes (Fig.1). We argue that the diffusive kinetics reveals the athermal nature of the structural rearrangements, the latter being driven by the global solvent flow itself (section IV B). Accordingly, we are led to describe syneresis as a calcium-fueled, closed-loop aggregation mechanism saturating at exhaustion of single egg-boxes. Finally (section IV C), we show that the syneretic process (*aging*) can be played backward (*rejuvenation*) by swelling the network using an osmotic shock.

II. MATERIALS AND METHODS

A. Alginate solutions

Sodium Alginate, isolated from *Lessenia nigrescens*, was purchased from Kalys S.A. (France) and used without further purification. Its nominal fraction of Guluronic acid is $FG = 0.45$. The pregel solutions were prepared as follow: Powder was first dispersed in water. The resulting lump was then allowed to swell for days under continuous stirring using a laboratory mixer until a homogeneous solution was obtained. Alginate concentrations used in this study were $C_A = 4$, 6 and 10 wt.%. Alternately one can express the amount of alginate in the pregel as the concentration of residues C_{res}. The molar mass of sodium uronates (M or G) being 256 Da, $C_{\text{res}} = 390$ mM in a $C_A = 10$ wt.% solution.

The entanglement concentration was previously determined[20] to be $C_E = 1$ wt. %. So, all the pregel solutions were in the entangled regime with Newtonian plateau viscosities ranging between 10^4 and 10^6 Pa.s.

B. Stopped-flow extrusion

An extrusion setup (see Fig.2) previously designed to study viscoelastic flow instabilities[20] was used to perform original "stopped-flow" extrusion experiments. Polymer solutions were filled into 1 mL syringes. The syringes were left at rest in order to degas. The remaining tiny bubbles were however useful as tracers materializing a portion of the gel. Using a syringe pump, the pregel solutions were extruded through capillaries of inner diameters $D_c = 200,\ 300,\ 500$ or 840 μm into a bath containing 60 mL of a solution of $CaCl_2$ (AnalaR NORMAPUR, VWR, France) of molar concentration c_0 ranging between 0 (deionised water) and 1 M. The whole setup, including the pregel syringe and the gelling bath, was enclosed in a temperature-controlled box at 20 ± 0.5°C.

The extrusion flow rate was chosen as high as possible while remaining in the stability domain of extrusion with respect to the visco-elastic helical instability[20]. The extruded pregel was therefore a cylindrical fibre of diameter D_0 ($D_0 > D_c$ due to viscoelastic swelling[21]). The piston drive was then suddenly stopped so as to "freeze" a portion of fibre in the field of view of a CCD camera. The fibre was observed under quasi-parallel illumination. The steep refractive index gradient associated with the gelation front was clearly visible. When

required, higher contrast was achieved by slightly defocussing the camera objective (see Supplementary Information Sec. 1 and movie). The diameter d_f of the cylindrical front was therefore determined accurately except at the end of the stage when the front reached the axis.

Thanks to the stopped-flow precedure at high flow rates (high Péclet numbers[3] ensuring negligible ion diffusion before stopping), we had access to the very beginning of the gelation process for which $d_f \simeq D_0$. This defined the origin of the time variable t_1 used to describe primary gelation. At $t_1 = t_g$ the front reached the fibre axis, marking the end of the primary gelation stage. Focus was then adjusted so as to subsequently measure the diameter D of the fibre with accuracy as a function of $t = t_1 - t_g$. Two tiny bubbles were picked in the field of view and subsequently tracked so as to materialize a fibre portion of length $L(t)$. The volume of this portion was computed as $V(t) = L(t)\pi D(t)^2/4$. Defining $V(t_g) = V_g$ the syneresis ratio $Q(t) < 1$ was computed as $Q(t) = V(t)/V_g$. The $\pm$ 2 pixel resolution on lengths measurements resulting typically in a $\pm 3\%$ uncertainty on Q.

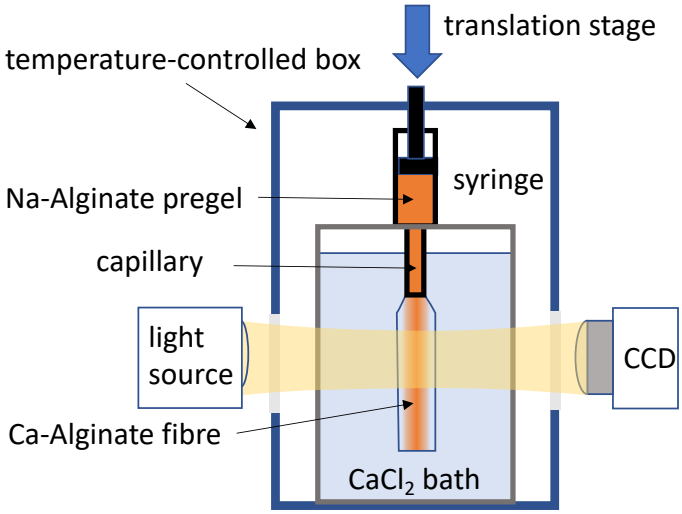

FIG. 2. Sketch of the stopped-flow extrusion setup. The pregel is pushed by a syringe pump held vertically and extruded through a capillary into a gelling bath containing Ca^{2+} ions. The whole setup is enclosed in a temperature-controlled box with transparent windows for observing the extrudate with a CCD camera under white light illumination.

[3] Péclet number $Pe = VD/\mathcal{D}_{\text{ion}}$ with V the fibre velocity and $\mathcal{D}_{\text{ion}}$ the diffusion coefficient of calcium ions in the gel.

III. RESULTS AND DATA ANALYSIS

As shown in Fig.3, a clear distinction can be made between a primary gelation stage and the syneresis one proper. In the first place, two bright lines, symmetrical with respect to the extruded fibre axis, propagate from the edges inwards. Optically, they reveal a steep radial gradient of refractive index attributable to a sharp, cylindrical calcium diffusion front. Structurally, it separates a gel shell from a pregel core, as evidenced by the buoyancy-induced motion of a bubble which materializes the front as a solid boundary (see Supplementary Information Sec. 1 and movie). In the following, the latter will therefore be referred to as the "gelation front". Its diameter $d_f(t_1)$ falls to zero at $t_1 = t_g$. In the mean time, the outer diameter D of the fibre shrinks by less than 5%. For $t_1 > t_f$, D further decreases by more than 20% while the fibre remains optically homogeneous.

This time separation prompts us to address the kinetics of both processes separately.

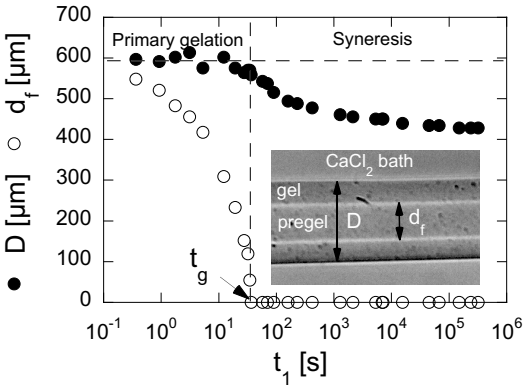

FIG. 3. Time-separation of the primary gelation and syneresis stages for a $C_A = 4$ wt.% pregel extruded in a in $c_0 = 100$ mM $CaCl_2$ bath through a $D_c = 500\,\mu$m glass capillary. The initial fibre diameter D_0 is larger than D_c due to viscoelastic swelling. During the *primary gelation* stage, a moving front of diameter $d_f(t_1)$ is clearly visible on the picture of the extrudate (inset). The gelation time $t_1 = t_g$ is defined when the front has reached the fibre axis. At this time, the fibre diameter D has not evolved significantly. The subsequent shrinking that corresponds to a slow decrease of D is described as *syneresis* proper.

A. Primary gelation stage

The gelation front appears as soon as the pregel is brought into contact with the gelling bath, i.e. right at the capillary exit. The extrusion velocity is chosen large enough for the gelation front to propagate but negligibly into the fibre before the extrusion is stopped. The diameter $d_f(t_1)$ of the gelation front is subsequently determined in a plane chosen at a distance from the capillary outlet larger than D_0 in order to minimize finite size effects. The origin of the timescale t_1 is determined precisely by tracking the measuring plane, materialized by an identifiable optical flaw, back to the capillary exit on the video recording.

The radial distance travelled by the front from the fibre edge is expressed in reduced form as: $\tilde{\rho}_f = 1 - d_f/D_0$. Its time evolution is plotted in Fig.4 for different values of c_0, the $CaCl_2$ concentration in the gelling bath. Two characteristic times can be extracted from the front kinetics: the time τ_g characterizing an initial regime fitted by $\tilde{\rho}_f(t_1) = \sqrt{2t_1/\tau_g}$ and the finite gelation time t_g at which the front reaches the fibre axis. Both τ_g and t_g decrease when the bath concentration c_0 is increased and increase with either the alginate content C_A or the fibre diameter D_0.

1. A minimal kinetic model

The natural framework for analysing the kinetics of calcium-induced gelation of alginate is that of reaction-diffusion processes[6]. The reaction involves calcium ions and G-blocks. The basic step is the formation of a calcium-bound dimer (egg-box), although the concomitant formation of higher order multimers has been evoked[7]. There is a consensus that gelation is diffusion-limited. Diffusion is primarily that of Ca^{2+} but the observation that gelation from an external calcium bath may lead to inhomogeneous samples has led to take free alginate chain diffusion into consideration. Chavez et al[5] have shown that trapping alginate pregel into a preformed thermoreversible gel (e.g. agar or gelatin) made it possible to analyse their data disregarding alginate chain motion. Here, we expect entanglements and self-crowding of the concentrated pregel solution to play the same role. We analyze our data with their simplified model, readily adapted to the cylindrical geometry (see Supplementary Information Sec. 2). It assumes that dimerisation is the sole reaction step relevant to the primary gelation stage. It is supposed quasi-instantaneous with respect to Ca^{2+} diffusion

(coefficient $\mathcal{D}_{\rm ion}$). This leads to a sharp gelation front where calcium concentration falls to zero.

An amount of n ions per unit volume is required to complete cross-linking. As long as $c_0 \ll n$, the front kinetics is slow enough for a quasi-stationary concentration profile to set up between the infinite bath of constant concentration c_0 at the fiber edge (diameter D_0) and $c = 0$ at the gelation front. This yields an implicit expression for the front diameter $d_f(t_1)$:

$$\frac{d_f^2}{2D_0^2}\left[\ln\left(\frac{d_f}{D_0}\right) - \frac{1}{2}\right] + \frac{1}{4} = \frac{c_0}{n}\frac{4\mathcal{D}_{\rm ion}t_1}{D_0^2}$$

which accounts qualitatively well for the observed front kinetics (see Fig.5). At short times, the reduced front diameter $\tilde{\rho}_f \sim \sqrt{2t_1/\tau_g}$ with:

$$\frac{D_0^2}{4\tau_g} = \mathcal{D}_{\rm ion}\frac{c_0}{n}$$

Gelation is completed ($d_f = 0$) in a finite time:

$$t_g = \tau_g/4$$

At larger bath concentrations ($c_0 > n$), the concentration profile is not in a steady state and must be computed numerically (see Supplementary Information Sec. 2). The initial regime can still be fitted by a square-root behavior. The characteristic time τ_g is however no longer linear in c_0. Namely:

$$\frac{D_0^2}{4\tau_g} = \mathcal{D}_{\rm ion} f\left(\frac{c_0}{n}\right) \tag{1}$$

$$\frac{t_g}{\tau_g} = \frac{1}{4} g\left(\frac{c_0}{n}\right) \tag{2}$$

with $f(x) \sim x$ in the $x \ll 1$ limit and $g(0) = 1$ so as to recover the quasi-stationary limit.

Under the hypothesis that the gel topology is independent of the alginate content in the entangled regime, n should be proportional to C_A. Accordingly, we have plotted D_0^2/τ_g and t_g/τ_g vs. c_0/C_A in Fig.5 for different values of the parameters. The collapse of the data along master curves is fully compatible with the scaling laws (1) and (2). Moreover, the computed (see Supplementary Information Sec. 2) function f fits remarkably well the data of main Fig.5 provided the free parameters $\mathcal{D}_{\rm ion}$ and n/C_A are given values $\mathcal{D}_{\rm ion} = 2.6 \times 10^{-10}$ m^2.s^{-1} and $n = 50$ mM for $C_A = 10$ wt.%, n being proportional to C_A. This strongly supports

the minimal hypotheses of the model: fixed alginate chains and second-order aggregation of G-blocks (egg-box cross-links)[4].

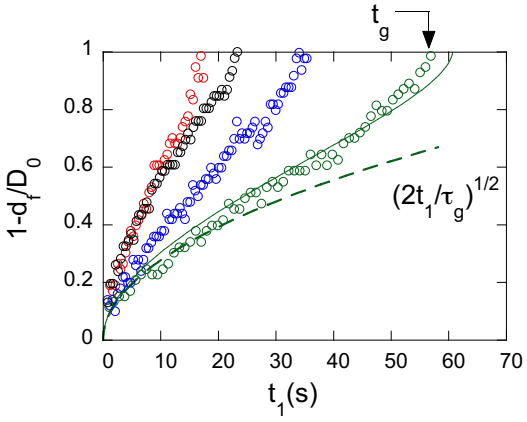

FIG. 4. Reduced distance travelled by the cylindrical gelation front of diameter d_f through pregel extrudates ($C_A = 10$ wt.%) of diameters $D_0 \simeq 520\,\mu$m in $CaCl_2$ gelling baths of concentrations: $c_0 = 100$, 250, 500, 1000 mM from bottom to top. The initial square-root of time regime (dashed line) defines the characteristic diffusion time τ_g. The full line is a fit of the slowest front position by the quasi-stationary solution of a simple reaction-diffusion model (see text). Completion of the primary gelation stage is achieved at $t_1 = t_g$.

The value obtained for $\mathcal{D}_{\rm ion}$ is of the same order of magnitude, though significantly smaller than the limiting value for self-diffusion in diluted $CaCl_2$ solution[22], an effect compatible with the slowing down of ion diffusion in concentrated electrolytes[22] or in the presence of highly charged polyelectrolytes[23]. In the following paragraph we discuss the value of n and make use of it to get insight into the network structure at the end of the primary gelation stage.

2. Strand length and network rigidity

The forthcoming analysis of the deswelling data (Sec.IV depends crucially on the nature of the network response to large deformations. Although alginate polymers are often referred to as "rigid", the Flory-Rehner model which assumes a gaussian (neo-hookean) elastic free

[4] The agreement of t_g/τ_g with the computed function g is poorer (see inset of Fig.5). This we attribute to the finite thickness of the gelation front (at least its optical trace) which leads to underestimate t_g.

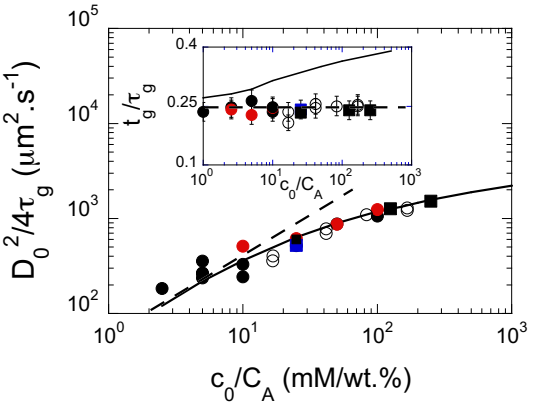

FIG. 5. Characteristics of the gelation front kinetics (diffusive time τ_g and gelation time t_g) for fibres of alginate fraction C_A(wt.%) (full squares: 4, open circles: 6, full circles: 10) and diameters D_0, extruded through capillaries of diameter $D_c(\mu\text{m})$ (blue: 200, black: 500, red: 840) in baths of concentrations c_0. Reduced variables c_0/C_A, $D_0^2/T\tau_g$ (main frame) and t_g/τ_g (inset) are dictated by the simple reaction-diffusion model described in the text. Solid lines are the numerical predictions. Dashed lines corresponds to the quasi-stationary limit of the model, obtained for small enough c_0/C_A.

energy has been recurrently used to interpret alginate hydrogel swelling[24–26], generally with unsatisfactory results. This section aims at evaluating the contour length $\mathcal{L}$ of polymer strands between neighbouring cross-links for our concentrated gels and to compare it to values of the persistence length ℓ_P found in the literature.

The amount n of calcium ions required to complete primary gelation was found proportional to the alginate concentration C_A. The concentration in G-residues in a $C_A = 10$ wt.% pregel is $FG \times C_{\text{res}} = 180$ mM. The stoechiometry of an egg-box being one chelated calcium ion per four residues, the pregel has the (maximal) capacity to bind 45 mM of Ca^{2+} ions. This value is close to the experimental value $n = 50$ mM suggesting that most of the G residues are involved in egg-box formation[5].

There is a consensus[4, 28, 29] that due to calcium-binding cooperativity, stable egg-boxes have a minimal length of about 20 G residues, i.e. 5 chelated calcium ions. Accordingly, we

[5] The situation is actually more complex since calcium ions can be prevented from bulk diffusion due to both specific chelation by G-blocks and Manning's condensation along the chains [27], thereby replacing the native sodium counterions of the pregel. A numerical estimate of the potentially condensed calcium ions (see Supplementary Information Sec. 3) is 130 mM, significantly larger than n. This strongly supports unexplained findings[16] that condensed sodium ions are not readily exchanged against calcium ones, so that n is mostly attributable to calcium ions chelated in the egg-box dimers.

estimate the density of cross-links in a 10 wt.% gel as $n_{\rm cl} = n/5 \simeq 10$ mM. Four strands emerge from a cross-link ; neglecting loops and dangling chains, each strand forms a link between two neighbouring egg-boxes. Their concentration is therefore $2n_{\rm cl}$. With a residue concentration $C_{\rm res} = 390$ mM, a polymer strand between two cross-links contains on average $C_{\rm res}/2n_{\rm cl} \simeq 20$ residues of length 0.45 nm. Finally, the average contour length of a strand in a 10 wt.% gel is $\mathcal{L} \simeq 9$ nm. Since $n \sim C_A \sim C_{\rm res}$ in the concentrated regime, our estimate of $\mathcal{L}$ which involves the ratio $C_{\rm res}/n$ does not depend on C_A.

Native alginate chains are rather stiff, a property they share with most biopolymers[18]. More precisely, the persistence length ℓ_p characterizing the loss of correlation in the orientation of monomers is much larger than the monomer (residue) size. Since alginate is a polyelectrolyte, its stiffness increases upon decreasing the ionic strength of the solvent. In the limit of infinite ionic strength and infinite dilution, the intrinsic persistence length[3] is $\ell_p = 12$ nm. In the entangled limit, ℓ_p is found independent of the alginate concentration and of the ionic strength and a conservative value in this regime[30] is $\ell_p = 15$ nm. Only polymer strands of contour lengths $\mathcal{L} \gg \ell_p$ will behave as gaussian ones. The estimated value $\mathcal{L} \simeq 9$ nm leads us to conclude that:

$$\mathcal{L} \simeq \xi < \ell_p$$

with ξ the network mesh-size (average distance between neighbouring cross-links). This regime corresponds to the so-called *semi-flexible* response of polymers[31] in which small deformations are accommodated by reducing the remaining strand entropy, while larger deformations require strand buckling and bending (they behave as more *rigid* filaments[32, 33]).

We have performed a control experiment so as to estimate directly the elastic response of an alginate fibre at the very end of the primary gelation phase. The fibre was first of all transferred to pure water then quickly fixed between the grips of a loading machine and submitted to a load-unload cycle at maximum strain 4% over a 10 s run (Fig.6). The response exhibits little non-linearity and hysteresis. The Young modulus $E = 2.7$ MPa corresponds to a shear modulus $G = E/3 \sim 1$ MPa. For the sake of comparison, the shear modulus of a gaussian network with no loop or dangling ends, i.e. with a density of elastically active strands proportional to the density of cross-links $n_{\rm cl}$ is $G \simeq 2n_{\rm cl}RT$. Our previous estimate, scaled to correspond to $C_A = 6$ wt.%, is $n_{\rm cl} \simeq 12$ mM hence $G \simeq 60$ kPa. This confirms

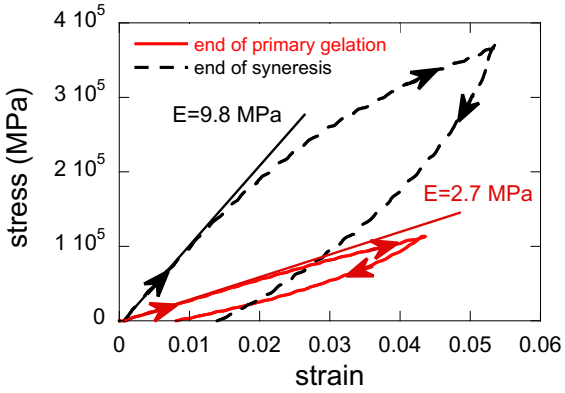

FIG. 6. Uniaxial stress-strain response of an alginate fibre (C_A = 10 wt.%, c_0 = 250 mM, D_c = 840 μm) just after the primary gelation stage (full red curve) and at saturation of syneresis (dashed black curve). Duration of the loading-unloading cycle is 10 s.

unambiguously that our densely cross-liked gels are made of stiff filamentous strands[1].

B. Syneresis

During syneresis, not only fiber diameters but also their lengths shrink. More precisely, Fig. 7 shows that the deswelling of a fibre portion is reasonably isotropic, as expected for the deswelling of an infinite and unconstrained cylinder of gel[36, 37]. Accordingly, and since syneresis starts to develop significantly only for $t_1 > t_g$, we define $t = t_1 - t_g$ and plot (Fig.8) the swelling ratio for a given cylindrical fibre portion:

$$Q(t) = \frac{V(t)}{V(0)} \tag{3}$$

where $V(0)$ is therefore its volume at the end of the primary gelation stage.

1. *Syneresis exhibits a wide spectrum of relaxation times*

As clearly illustrated in Fig.8, syneresis is an ultra-slow, saturating process. Its long-tailed nature was overlooked in previous studies[17] due to the choice of a *linear* time scale

[1] This is compatible with the finding[34, 35] that the elastic modulus of densely cross-linked alginate gels does not follow the entropic, rubber elasticity prediction but rather shows a significant enthalpic contribution compatible with a rigid filamentary network. Likewise, the standard Flory-Rehner theory has been found unable to account for the dependence of the equilibrium swelling ratio on the number of polymeric unit between crosslinks of calcium-limited alginate gels[26].

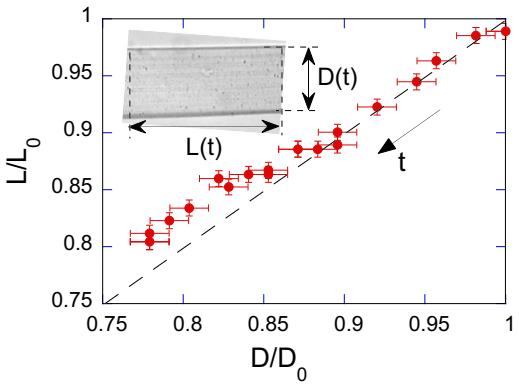

FIG. 7. Radial vs. longitudinal shrinkage during syneresis of a portion of gel (C_A = 4 wt.%, c_0 = 100 mM) of initial diameter D_0 and length L_0 (inset). $L(t)/L_0$ and $D(t)/D_0$ decrease as time t increases. The dashed line corresponds to the isotropic deswelling predicted by linear poroelasticity (see text).

for plotting $Q(t)$. Using a *logarithmic* timescale and correlatively extending the duration of observation reveals a dynamics spanning more than six decades of time. Deswelling gradually slows down (on a log scale, hence the "ultra"-slow qualifier) until approaching a apparent saturation value Q_∞ asymptotically. A single exponential decay is unable to fit the data. The long-tailed evolution is reasonably accounted for by a Kohlrausch function :

$$Q(t) = Q_\infty + (1 - Q_\infty) \exp\left[-(t/\tau)^\alpha\right] \tag{4}$$

indicating that syneresis involves a wide spectrum of relaxation times. A best fit of the data of Fig.8 yields $\alpha = 0.4$, i.e. the decay of Q is of the "stretched exponential" type ($\alpha < 1$) frequently met in slow relaxation processes in glasses. Although the stretched exponential fails to catch accurately the very beginning of syneresis it accounts well for 80% of the long-tailed relaxation and provides with a convenient way to define a characteristic time τ, the width of the relaxation spectrum being embedded into the exponent α[38].

In the following, for the sake of avoiding uncertainties associated with multiparameter, non-linear fits, we will characterize syneresis by Q_∞ and τ only, the exponent α remaining fixed to 0.4 a value which provides a satisfactory fit of all the data (Fig.10.a).

Thus, at this point, we have reduced the characterisation of syneresis to Q_∞ and τ. Establishing their dependence with respect to c_0, C_A, and D_0 remains a formidable task,

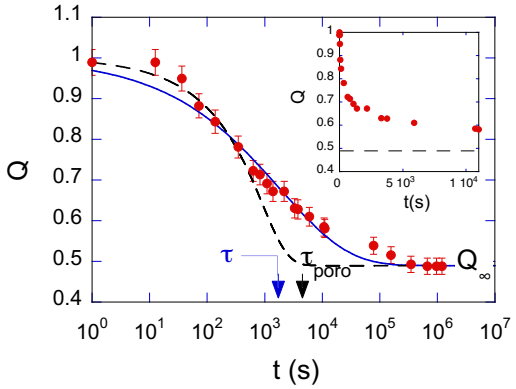

FIG. 8. Swelling ratio Q of a gel fiber portion ($C_A = 4$wt.%, $c_0 = 100$mM, $D_0 = 890\,\mu$m) at a time t after completion of the primary gelation stage. The logarithmic time scale reveals the wide relaxation time spectrum of the syneresis process which extends over more than 5 decades of time before slowing down and plateauing at a ratio Q_∞. Full line is a fit by a stretched exponential (4) with parameters $Q_\infty = 0.49 \pm 0.005$, $\tau = 1620 \pm 140$ s, $\alpha = 0.4 \pm 0.03$. Dashed curve corresponds to the poroelastic solution for deswelling after an osmotic shock corresponding to an equilibrium swelling ratio Q_∞ (see IV B) with a poroelastic time $\tau_{\rm poro} = 4000$ s adjusted to fit the initial $Q(t)$. Inset: Same data as main figure plotted using a *linear* time-scale stopped after a few τ. The long-tailed nature of the relaxation is missed and the apparent saturation level ($\simeq 0.6$) is largely overestimated.

especially in view of the prohibitive time required to reach saturation systematically. Rather than carrying out a genuine multidimensional mapping, we have studied $Q_\infty(C_A)$ at constant c_A and D_0, and $\tau(D_0)$ at constant c_0 and C_A. The calcium concentration c_0 being a key parameter controlling the kinetics of primary gelation, its role in syneresis deserved a specific test. This was addressed via an experimental procedure referred to as "solvent-swap experiment" (Sec. III B 4).

2. *Syneresis saturates at a "magic" ratio 1/2*

Let us first of all focus on Q_∞ which characterizes what appears to be the completion of the syneresis process. Note that due to the ultra-slowness of the decay we cannot exclude that, for unreachable long times, deswelling may resume after a transient plateau. Keeping this

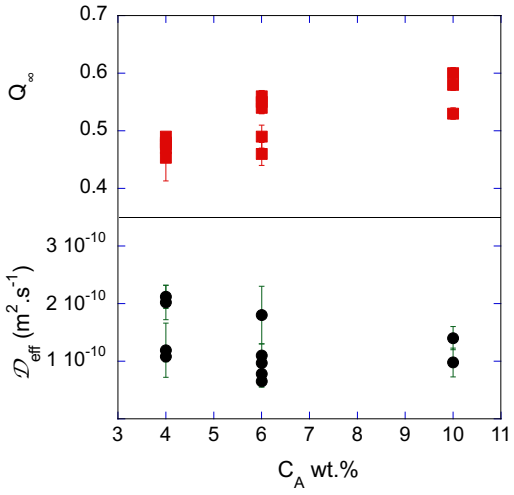

FIG. 9. Effect of the alginate content C_A on the kinetics of syneresis for fibres extruded in a $c_0 = 100$mM calcium bath through a $D_c = 500\,\mu$m, capillary. Upper panel: Swelling ratio at saturation Q_∞ Lower panel: Apparent diffusive coefficient $\mathcal{D}_{\rm eff}$.

in mind, we will however refer to Q_∞ as the "saturation" value for the sake of convenience.

Our key result, illustrated by Fig.9.a, is that Q_∞ depends but weakly on C_A. As a rule of thumb, *syneresis reaches an apparent saturation when the fibre volume has been halved,* i.e. $Q_\infty \simeq 1/2$. In view of the scattered values reported in the existing literature, this appears to be a specificity of our densely cross-linked gels. In the following discussion (sec. IV) we will argue that the "zeroth order" 1/2 ratio is a strong indicator of the underlying structural process, hence the somewhat provocative "magic" qualification. At next order, Q_∞ increases weakly with C_A, i.e. self-crowding tends to limit syneresis.

3. Syneresis is a diffusive process

The fact that a single characteristic time τ is sufficient to describe the long-tailed relaxation prompts us to define a reduced time scale:

$$t^* = \frac{t}{\tau} \tag{5}$$

Accordingly, when plotting Q with respect to t^*, data that correspond to diameters D_0

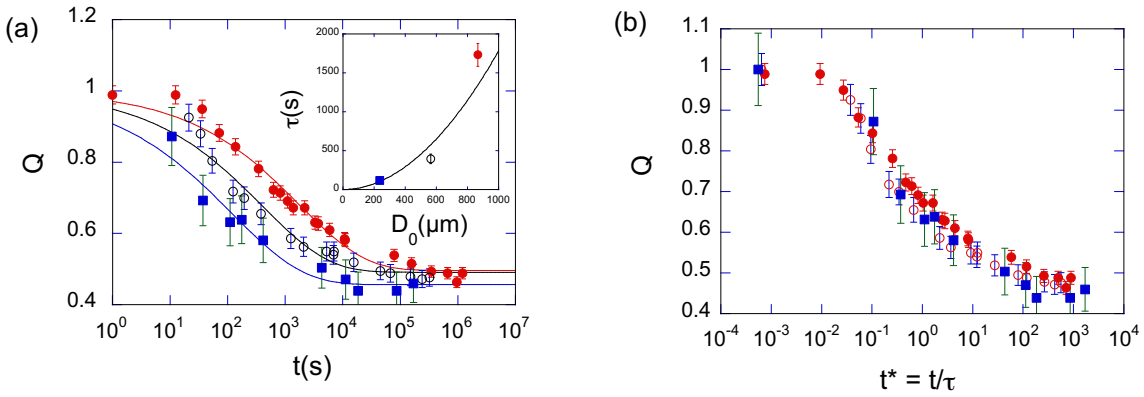

FIG. 10. (a) Role of the initial diameter D_0 on the kinetics of syneresis of $C_A = 4$ wt.% in $c_0 = 100$mM calcium-alginate gels. $D_0 = 240\,\mu$m (filled square), $560\,\mu$m (open circle) and $870\,\mu$m (filled circle). Full lines are fits by stretched exponential functions (4) with a fixed exponent $\alpha = 0.4$ but free values of Q_∞ and τ. Inset: Plot of $\tau(D_0)$. The data are compatible with a diffusive bahavior (quadratic fit). (b) Same data as (a) plotted with respect to $t^* = t/\tau$ showing their collapse on a master curve over the *whole* syneresis process, spanning 6 decades in reduced time.

spanning a four-fold range (same alginate and calcium concentrations) collapse on a single, stretched exponential master curve over more than 6 decades of reduced time (Fig.10.b).

The characteristic times τ increase quadratically with the fibre diameter D_0 (see inset of Fig.10.a), pointing undoubtedly to a *diffusive* origin with an effective diffusion coefficient $\mathcal{D}_{\rm eff}$ defined by:

$$\tau = \frac{D_0^2}{4\mathcal{D}_{\rm eff}} \tag{6}$$

Fig.9.b shows that $\mathcal{D}_{\rm eff} \simeq 1$–$2 \times 10^{-10}$ m^2.s^{-1}, slightly decreasing as C_A increases. Although finding $\mathcal{D}_{\rm eff}$ of the order $\mathcal{D}_{\rm ion}$ might lead to deduce that calcium diffusion controls syneresis like in the primary gelation stage, next section will rule this possibility out by showing that, in a wide range of calcium concentration, calcium uptake is not a factor limiting the kinetics of syneresis, leaving network/solvent relative motion as the more likely candidate to the underlying diffusive mechanism.

4. A solvent-swap experiment

Here we report on an experimental protocol specifically designed to assess the role of calcium ion concentration on the kinetics of syneresis, including values of c_0 too low for primary gelation to be completed before alginate molecules have started dissolving in the bath. In these experiments, primary gelation and syneresis were first of all left to proceed the usual way in a $c_0 = 1$M bath. At $t^* \simeq 0.25$ ($t \simeq 100$ s) the gelling bath was swapped for a bath of lower concentration $c_{\rm swap}$. Taking into account the finite time required for swapping baths and the diffusive time for calcium concentration to equilibrate across the fibre, one can consider that for $t^* > 1$ the network relaxation is controlled by the new calcium concentration. We subsequently measured the ratio $Q(t^*)$ for several decades of time.

Fig.11 reveals two regimes, depending on the calcium concentration $c_{\rm swap}$:

(i) For $c_{\rm swap} \geq 10$ mM, syneresis resumes apparently unperturbated, i.e. it follow closely the reference curve $Q^{\rm ref}(t^*)$ obtained with $c_0 = 1$ M. We will refer to this regime as the "calcium-saturated" one. Its existence shows that the supply of binding ions does not limit syneresis. This leaves *poroelasticity* as the sole relevant diffusive mechanism at stake. Poroelasticity refers to the coupling between the water chemical potential (or pore-pressure, the gradient of which induces solvent flow) and the network elastic deformations[39]. In the linear response limit, it leads to a diffusive relaxation process, the motion of the solvent relative to the deformable network being ruled by a "collective" diffusion coefficient $\mathcal{D}_{\rm coll}$ which depends on the solvent viscosity, the effective pore size $\sim \xi$, the network shear modulus G and the Poisson ratio[6] ν. The central role played by the poroelastic flow on the syneresis dynamics will be discussed at length in section IV B.

(ii) For $c_{\rm swap} \leq 1$ mM syneresis is hindered, i.e. after some time lag compatible with the ion diffusion through the fibre, deswelling stops. In the pure water case ($c_{\rm swap} = 0$), some positive swelling is observed. This regime is compatible with previous observations[17] that the level of syneresis Q_∞ increases with calcium concentration until plateauing at a concentration-independent value for concentrations larger than, typically 20 mM.

Once the solvent bath has been swapped, the concentration of calcium ions *inside* the gel reaches a value, larger than $c_{\rm swap}$, fixed by the global electro-neutrality of the gel and

[6] ν is defined in the "drained" state, i.e. when solvent flow has relaxed pressure gradients (in the "undrained" state, the Poisson ratio is 0.5). Since shear induces no volume change, it does not couple to the solvent flow and G has the same value under drained or undrained conditions.

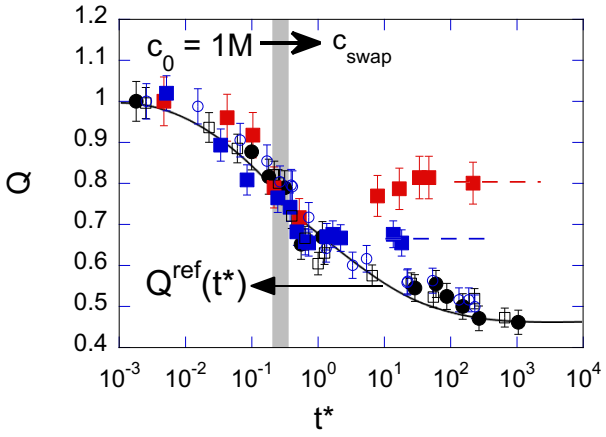

FIG. 11. Solvent swap experiment. Filled black circles are the reference syneresis data $Q^{\mathrm{ref}}(t^*)$ for $C_A = 6$ wt.%, $c_0 = 1000$ mM and $D_c = 500\,\mu$m (black line is a guide for the eyes). Other symbols corresponds to a solvent swapping against $CaCl_2$ baths of concentration $c_{\mathrm{swap}} = 0$ (pure water, filled red squares), 1 (filled blue squares), 10 (open squares) and 100 mM (open circles). The finite time required for swapping baths is indicated by the width of the greyed zone. Data corresponding to pure water and $c_{\mathrm{swap}} = 1$ mM depart from the reference data. The corresponding saturation levels are indicated by dashed lines. At higher concentrations, the course of syneresis remains unaffected by the solvent swap.

the absence of mobility of the network-bound charges (Donnan equilibrium[40]). The concentration difference results in a net osmotic pressure $\Delta\Pi_{\mathrm{ion}}$ which tends to swell the gel. A key factor is c_{b} the concentration of network bound charges uncompensated by Manning counterion condensation and chelation. Assuming that sodium ions, including the primarily condensed ones, have been ultimately permuted against calcium ions, one estimates (see Supplementary Information Sec. 3) $c_b \simeq 30$ mM for the $C_A = 6$ wt.% gel. As long as $c_{\mathrm{swap}} \gg c_{\mathrm{b}}$, the counterion imbalance is negligible and $\Delta\Pi_{\mathrm{ion}} \simeq 0$. When $c_{\mathrm{swap}} \ll c_{\mathrm{b}}$ however, most counterions remains trapped inside the gel and $\Delta\Pi_{\mathrm{ion}}$ grows to a level responsible for the super-absorbent power of ionic gels. The limiting law expression (when activity equals concentration) for the swelling pressure in that case is $\Delta\Pi_{\mathrm{ion}} = c_{\mathrm{min}}RT$ with R the Mayer constant. For $C_A = 6$ wt.% this reads $\Delta\Pi_{\mathrm{ion}} = 75$ kPa. The response of the gel to this osmotic pressure will be discussed in the next section.

IV. DISCUSSION OF A MINIMAL SCENARIO

The systematic study of syneresis in concentrated alginate gels has, quite unexpectedly, revealed some simple and robust features regarding both the kinetics of deswelling and the apparent saturation reached at long times. In line with the credo that a simple behavior should have a simple physical origin, we aim at proposing a minimal scenario for syneresis in the strongly entangled limit, compatible with experiments and incorporating the structural idiosyncrasies of alginate gels, namely the rigidity of their networks and their capability to change topology (cross-link number and connectivity) via calcium-induced egg-box aggregation.

The questions we have to answer are the following :

(i) What is the nature of the coupling between the local network rearrangements and the observed global flow that can explain Q_∞?

(ii) What is the statistical nature of the network restructuration that can conciliate random local events with a dynamics fully controlled by the average diffusive time for global deswelling?

Point (i) will be addressed in IV A and point (ii) in IV B.

A. Magic ratio 1/2: insight into the elementary structural events responsible for syneresis

The narrow range of deswelling ratios at saturation (Fig.9) is in contradistinction with the scattered nature of the previously published data[12, 13, 17]. In the densely cross-linked gels under study, syneresis saturates when the initial fibre volume has been halved. It is tempting to try and ascribe this "magic" ratio $Q_\infty = 1/2$ to a mere geometrical feature, irrespective of physico-chemical details.

The fact that Q saturates indicates that the network has reached a quasi-stationary state with respect to both changes in the strand lengths and in the number and connectivity of cross-linking G-block aggregates. At this point of the discussion it is useful to clearly distinguish between (de)swelling at fixed network connectivity e.g. in response to a solvent quality modification, and volume change associated with the physical network rearrange-

ment. Whereas in the first case (referred to in the following as "elastic swelling"), volume change is accommodated by strand elastic deformation only, in the second case, it involves the plastic events responsible for the structural evolution. The common belief about syneresis is that it pertains to the second case. However, the mechanism coupling the network rearrangement and the solvent flow needs to be clarified.

1. Plastic events are responsible for solvent release

Due to changes in network connectivity, the syneresis equilibrium problem is far more complex than the elastic deswelling one since any structural change resets the elastic reference state of the network. The theoretical formulation of the problem, usually referred to as "permanent set" in rubber theory[41], leaves but few expectation regarding a C_A-independent value of Q_∞. Actually, the elastic free energy (and the elastic pressure) depends not only on the current swelling ratio but also on the full swelling and cross-linking history. Each time aggregation occurs, the gel relaxes (deswells) so as to balance the osmotic and elastic pressures. Thus Q_∞ depends crucially on the elastic response of the network (its osmotic compressibility) at each cross-linking level. We therefore propose that the previously discussed strand rigidity plays a crucial role by fixing the average distance ξ between cross-links (themselves of lengths of order ξ), whatever their aggregation state.

In such an open cell, rigid cellular network picture, the sample volume V is related to the number of cross-links $N_{\rm cl}$ via $V = N_{\rm cl}\Omega$ with $\Omega \sim \xi^3$ the volume of a unit cell. Within this infinitely stiff limit, the equilibrium elastic pressure $\Pi_{\rm el}$ is a mere Lagrange multiplier enforcing the volume conservation. Since the stacking of two neighbouring cross-links, corresponding to the plastic collapse of a unit cell, induces the draining-out of a volume Ω of solvent, Q is simply fixed by the geometrical relationship between the sample volume and the number of cross-link. The syneresis ratio reads at any time:

$$Q(t) = \frac{N_{\rm cl}(t)}{N_{\rm cl}(0)} \tag{7}$$

This picture is compatible with $Q_\infty = 1/2$ provided that the elementary structural event responsible for syneresis is the *binary* stacking of egg-boxes and that saturation corresponds to the exhaustion of all available neighbouring primary cross-link pairs.

Further aggregation, involving higher order of stacking, could occur in principle[16] but is

certainly dramatically slowed down by topological constraints (entanglements but also the increasing network connectivity), network stiffness and self-crowding. However as shown in fig.9 Q_∞ is slightly smaller than 0.5 for the less concentrated gels ($C_A = 4$ wt/%). This is a hint that further aggregation have started in these gels. On the opposite, $C_A = 10$ wt.% gels do not reach $Q_\infty = 0.5$, an indication that the full completion of binary box aggregation is prevented in the most crowded gels.

2. Quantitative support from the solvent-swap experiments

In order to support our phenomenological description based on an infinitely rigid network subject to plastic events (cell collapse), let us further consider the outcome of the solvent-swap experiment (section III B 4), namely that syneresis can be stopped by a solvent of low enough calcium concentration. A natural interpretation is that, in this case, the swelling pressure $\Delta\Pi_{\rm ion}$ counteracts the syneretic deswelling force, i.e. hinders the stacking of egg-box cross-links.

In a bath at $c_{\rm swap} = 1$ mM $\ll c_b$, the osmotic pressure corresponding to the Donnan equilibrium remains close to $\Pi_{\rm ion} \simeq 75$ kPa estimated in section III B 4 for $c_{\rm swap} = 0$. Since no syneresis nor swelling is observed in that solvent, one can consider that the virtual work against a stacking event $\Delta\Pi_{\rm ion}\Omega$, with $\Omega \sim \xi^3$ the volume of a unit network cell, balances the gain in free energy $5\Delta G_{\rm b}$ corresponding to the calcium-induced binding, 5 being the estimated average number of calcium ions per egg-box and $\Delta G_{\rm b}$ the free energy of chelation for a single ion. With $\xi \simeq 10$ nm, one gets $\Delta G_{\rm b} \sim 0.1$ eV/ion, a reasonable order of magnitude for calcium binding[42].

This corroborates our picture of a rigid network for which volume cannot change significantly but via plastic egg-box rearrangements. This is confirmed by submitting a fibre left for 10^5 s in a 250 mM calcium bath to uniaxial tensile loading (Fig.6). The response to the load/unload test exhibits a large hysteresis and some marked softening even at small strains. This is fully compatible with the disruption of weaker secondary cross-links, the formation of which is revealed by the value of the Young modulus (9.8 MPa) at vanishing loading strains, significantly higher than the modulus (2.7 MPa) prior to syneresis.

Interestingly, calcium ions are responsible for antagonistic effects: their entropy controls the swelling osmotic pressure while their binding energy favors G-block aggregation hence

induces deswelling. Thus, tuning the amount of calcium ions in the gel environment makes it possible to control syneresis, i.e. to stop it or even to reverse it to some extent;

B. Network rigidity enslaves *local* collapse events to *global* solvent flow.

Let us now address the dynamical aspects of syneresis. As discussed previously, syneresis is not just elastic deswelling since it is driven by the slow, calcium-induced collapse events. Solvent flow at times much shorter than the characteristic time of the stretched exponential ($t \ll \tau$) can however be considered to occur at essentially fixed network structure.

The isotropic, elastic (de)swelling of an infinite, unconstrained cylinder has deserved several theoretical studies[36, 37]. The transient swelling ratio towards the equilibrium value Q_∞ reads:

$$Q_{\rm poro}(t) = Q_\infty \Psi(t/\tau_{\rm poro}) \tag{8}$$

where Ψ depends only on the drained network Poisson's ratio ν and where the poroelastic time is:

$$\tau_{\rm poro} = D_0^2/(4\mathcal{D}_{\rm coll}) \tag{9}$$

We have computed an approximate [36] but accurate[37] analytical solution for Ψ, setting quite arbitrarily $\nu = 0$. The value of $\tau_{\rm poro}$ was adjusted to fit the *initial* shrinking phase (Fig.7). The corresponding collective diffusion coefficient is $\mathcal{D}_{\rm coll} \simeq 5 \times 10^{-11}$ m^2.s^{-1}, a typical order of magnitude for concentrated physical gels[43]. As a matter of fact, $\tau_{\rm poro}$ is found on the order of the characteristic time τ of the stretched exponential ($\tau_{\rm poro} \simeq 3\tau$), suggesting that both times, hence the two diffusive processes have the same physical origin. Accordingly, we will keep on characterizing the relaxation spectrum by τ but refer to it as the "poroelastic time".

Despite the fact that they share the same characteristic time scale, neither one of the two test functions is able to fit the relaxation over the whole time window. Actually they are complementary: while the stretched exponential fails to fit the initial phase of syneresis, the poroelastic solution is unable to account for the long tail of the volume relaxation.

The existence of a long tail dynamics is typical of relaxation in disordered systems. Here, a natural expectation would be as follows. Due to the uneven distribution of G-blocks along the alginate chains, the network is likely to show frozen fluctuations of cross-link density and strand length. Some egg-box pairs are able to stack on the spot while most others require

significant relative displacements for calcium-induced binding to proceed. This translates to a wide distribution of energy barriers. Classically, a thermally-activated dynamics over this energy landscape results in a wide relaxation spectrum, responsible for a quasi-logarithmic or strongly stretched dynamics, *independent of the sample size*. Scaling time by D_0^2 would result in a collapse of the short time ($t \ll \tau_{\rm poro}$) part of the relaxations curves, leaving the tail separation unaffected (a situation akin to visco-elasto-plastic stress relaxation of hydrogels[44, 45]). Fig.10 clearly indicates that such is not the case in the present study.

We are therefore led to conclude that egg-box aggregation in self-crowded gels is an *athermal* process, i.e. that thermal activation is essentially irrelevant. Many jammed systems pertaining to the "soft glassy materials" class (dense emulsions, pastes, foams, gels,...) are athermal. Nevertheless, they generally exhibit slow relaxations (aging) when prepared in an out-of-equilibrium state. This is attributed[46] to some "mechanical noise" resulting from the accumulation of elastic signals sent by individual rearrangement events which in turn trigger new events remotely.

Taking into account the biphasic nature of hydrogels, we propose to complete our scenario as follows: cell collapse events send pore-pressure signals that relax diffusively via poro-elastic movements of solvent. Their build-up leads to the global syneretic flow. In turn, due to frozen inhomogeneities, the average network shrinking results in non-affine deformations, locally far enough from the average level to be able to trigger new egg-box aggregations. Although the deswelling flow is deterministic, due to frozen disorder, these events occur *at random times*. In this picture, although the distribution of barrier heights remains responsible for the stretched nature of the decay, the time clock for the landscape exploration is provided by the global poroelastic time. It entails that structural relaxations are fully enslaved to the draining itself. The self-sustained process must start from these few places where egg-boxes are close enough for their stacking to proceeds spontaneously due to thermal noise and to the remaining entropy of the semi-flexible strands

C. Rejuvenation

Along this study we have analysed the syneresis of calcium alginate gels as an *aging* process, i.e. a spontaneous restructuration following the sample preparation (here, the end of the primary gelation stage). Like their harder counterparts, soft glassy materials generally

exhibit aging of their physical properties[47] (rheological response, correlation functions, ...). Unsurprisingly, when dealing with *soft* matter, aging shows a great sensitivity to the mechanical stresses[48]. Although shearing can lead to an enhancement of the process (overaging) in the first place, as the level of applied stress is increased it usually give rise to *rejuvenation*[49]: the structural build-up is partially destroyed and the system is set back to some anterior state. The stress/aging coupling is a fruitful indicator of the restructuring events at stake.

In order to assess whether swelling of aged gels can lead to their rejuvenation, we have complemented the solvent-swap experiment, in the case of swapping $c_0 = 1$ M for water, which results in positive swelling. As shown in Fig.12.a, we have changed the solvent back to its primary concentration at time t_f^*. At this time the ratio Q had reached a level Q_f, resulting from calcium-induced deswelling in the first place followed by some partial reswelling due to Donnan equilibrium in water. Since $Q_f < 1$ one can find an "age" t_i^* during the initial syneretic phase so that $Q(t_i^*) = Q_f$.

The states of the gel at t_i^* and t_f^* result from very different histories (fast deswelling up to $t_i^* \simeq 1$ on the one hand and slow reswelling up to $t_f^* \simeq 10$ on the other) driven by distinct forces (calcium binding or osmotic pressure due to free calcium ions). One may wonder if both states, beyond their common volume, share some microscopic, structural similarities that would justify the term "rejuvenation". Actually, when the solvent is swapped back to the original 1M concentration, the gel resumes syneresis. In order to compare it to the original deswelling $Q(t^* > t_i^*)$, we have plotted the evolution of the swelling ratio for $t^* > t_f^*$ time-shifted backward by $\Delta t^* = t_f^* - t_i^*$. By construction, both data start from the same point. Fig.12.b shows that, remarkably, they follow the same subsequent evolution within experimental error.

Thus, the swelling phase has reset the system into an anterior state. This means that beyond sharing the same volume, both networks are statistically equivalent with the same distribution of energy barrier heights which must be wiped out by the poroelastic flow in order to trigger stacking events. Due to network frozen-in (density, strand orientation, ...) fluctuations, stacking events proceed sequentially as Q decreases; the last cross-link to be formed being the more constrained. *Almost perfect rejuvenation* is striking and suggests that swelling disrupts these binary egg-box aggregates in reverse order with no randomizing noise source but the network frozen disorder itself. The fact that the kinetics of rejuvenation is irrelevant (here reverse swelling is much slower then the initial syneresis stage) confirms

that the kinetics of syneresis is fully encoded into the current cross-link distribution and that there is no internal clock but the poro-elastic one.

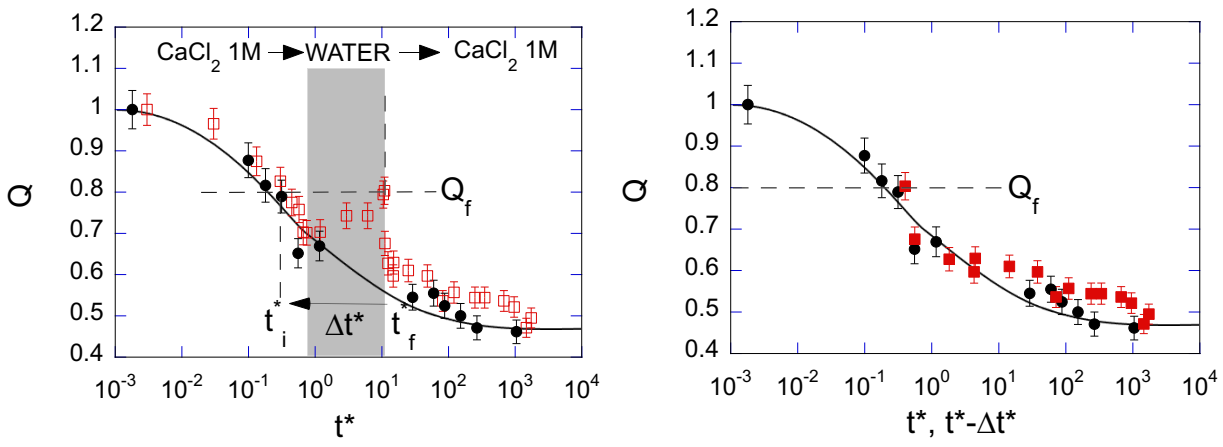

FIG. 12. Swelling-induced rejuvenation experiment. a. Black full circles and curve: same reference data is in Fig.11. Open red squares: the initial bath ($c_0 = 1$ M) is first swapped against pure water (greyed zone), inducing swelling up to a ratio Q_f (this ratio was first reached during syneresis at age $t^* = t_i^*$). At $t^* = t_f^*$ the solvent is swapped back to $c_0 = 1$ M: syneresis resumes. b. Full red squares: data subset ($t^* > t_f^*$) shifted by $\Delta t^* = t_f^* - t_i^*$ (note that in log scale the shift is not a mere translation). The shifted data collapse with the reference ones.

V. CONCLUDING REMARKS

Using a set of original macroscopic experiments we have provided the first complete scenario for syneresis in calcium-alginate hydrogels. It applies specifically to self-crowded, densely cross-linked gels which behave as stiff filamentous networks. We describe syneresis as an athermal aging process during which egg-box stacking events that induce solvent motion are triggered by the global deswelling flow itself. Such a closed-loop dynamics, paced by the poroelastic time for pore pressure relaxation over the whole sample, represents a paradigm shift inasmuch as deswelling is not a mere elastic response to an internal, calcium-fueled, noise-activated motor, as in most aging processes. As such, we think that syneresis in calcium-alginate, in addition of being of great relevance to applications, deserves further investigation as an original dynamical process in soft glassy materials.

The reported experiments are based on the measurement of the global deswelling ra-

tio; accordingly they provide no insight into the details of the flow-mediated correlations between events, during syneretic aging and swelling-induced rejuvenation. Diffusing-wave spectroscopy would be a suitable tool to investigate this point. It has been used in experiments with alginate gels less concentrated than ours, either in calcium limited experiments for which few syneresis is expected[47] or in external diffusion gelation in a large linear sample for which primary gelation and syneresis occurred concomitantly, leading to a surprising and still unexplained constant velocity gelation front kinetics[50]. Therefore, it is difficult to draw a parallel between these studies and the present one. However, it would be very interesting to revisit these seminal works in order to investigate the nature of the restructuring modes responsable for syneresis in the light of our findings and, in particular, to connect the reported "complex aging behavior, characterized by a strongly heterogeneous microscopic dynamics involving both local rearrangements persisting over very long time, and collective restructuring effects evidenced by sudden de-correlation bursts"[50] with the dynamics of syneresis proper.

Our scenario paves the way to a more detailed theoretical model based on numerical simulation of the deswelling of disordered filamentous networks with reversible cross-linking[51]. Taking into account the biphasic nature of the gel, however, is certainly challenging.

Finally, we hope that this study will contribute to establish the fruitful connection between a long-known engineering process and several active fields in soft matter physics such as the mechanics of stiff biopolymer network, aging in soft glassy materials and non-linear poroelasticity of highly deformable gels[52].

ACKNOWLEDGEMENTS

We are deeply indebted to Christiane Caroli for challenging discussions about aging and rejuvenation.

---

[1] K. Y. Lee and D. J. Mooney, Progress in polymer science **37**, 106 (2012).

[2] G. Grant, E. Morris, D. Rees, *et al.*, Febs Lett **32**, l (1973).

[3] I. Donati and S. Paoletti, in *Alginates: biology and applications* (Springer, 2009) pp. 1–53.

[4] I. Braccini and S. Pérez, Biomacromolecules **2**, 1089 (2001).

[5] M. S. Chavez, J. A. Luna, and R. L. Garrote, Journal of food science **59**, 1108 (1994).

[6] A. Mikkelsen and A. Elgsaeter, Biopolymers: Original Research on Biomolecules **36**, 17 (1995).

[7] T. Braschler, A. Valero, L. Colella, K. Pataky, J. Brugger, and P. Renaud, Analytical chemistry **83**, 2234 (2011).

[8] D. M. Kirchmajer, R. Gorkin Iii, *et al.*, Journal of Materials Chemistry B **3**, 4105 (2015).

[9] S. H. Bjørnøy, S. Mandaric, D. C. Bassett, A. K. Åslund, S. Ucar, J.-P. Andreassen, B. L. Strand, and P. Sikorski, Acta biomaterialia **44**, 243 (2016).

[10] Y. Jun, E. Kang, S. Chae, and S.-H. Lee, Lab on a Chip **14**, 2145 (2014).

[11] O. Bonhomme, J. Leng, and A. Colin, Soft Matter **8**, 10641 (2012).

[12] K. I. Draget, K. Østgaard, and O. Smidsrød, Carbohydrate polymers **14**, 159 (1990).

[13] K. I. Draget, O. Gåserød, I. Aune, P. O. Andersen, B. Storbakken, B. T. Stokke, and O. Smidsrød, Food Hydrocolloids **15**, 485 (2001).

[14] T. Van Vliet and P. Walstra, in *Water in Foods* (Elsevier, 1994) pp. 75–88.

[15] T. Divoux, B. Mao, and P. Snabre, Soft Matter **11**, 3677 (2015).

[16] Y. Fang, S. Al-Assaf, G. O. Phillips, K. Nishinari, T. Funami, P. A. Williams, and L. Li, The Journal of Physical Chemistry B **111**, 2456 (2007).

[17] A. Martinsen, G. Skjåk-Bræk, and O. Smidsrød, Biotechnology and bioengineering **33**, 79 (1989).

[18] C. Storm, J. J. Pastore, F. C. MacKintosh, T. C. Lubensky, and P. A. Janmey, Nature **435**, 191 (2005).

[19] Y. A. Mørch, S. Holtan, I. Donati, B. Strand, and G. Skjåk-Bræk, Biomacromolecules **9**, 2360 (2008).

[20] L. Picaut, O. Ronsin, C. Caroli, and T. Baumberger, Physical Review Fluids **2**, 083303 (2017).

[21] R. Tanner, Journal of Polymer Science Part A-2: Polymer Physics **8**, 2067 (1970).

[22] J. H. Wang, Journal of the American Chemical Society **75**, 1769 (1953).

[23] G. S. Manning, The Journal of Chemical Physics **51**, 934 (1969).

[24] S. T. Moe, G. Skjaak-Braek, A. Elgsaeter, and O. Smidsroed, Macromolecules **26**, 3589 (1993).

[25] K. Y. Lee, J. A. Rowley, P. Eiselt, E. M. Moy, K. H. Bouhadir, and D. J. Mooney, Macromolecules **33**, 4291 (2000).

[26] M. Davidovich-Pinhas and H. Bianco-Peled, Carbohydrate Polymers **79**, 1020 (2010).

[27] I. Donati, J. C. Benegas, A. Cesàro, and S. Paoletti, Biomacromolecules **7**, 1587 (2006).

[28] K. Draget, M. Simensen, E. Onsøyen, and O. Smidsrød, in *Fourteenth International Seaweed Symposium* (Springer, 1993) pp. 563–569.

[29] B. T. Stokke, O. Smidsroed, P. Bruheim, and G. Skjaak-Braek, Macromolecules **24**, 4637 (1991).

[30] B. Maciel, C. Oelschlaeger, and N. Willenbacher, Colloid and Polymer Science **298**, 791 (2020).

[31] C. P. Broedersz and F. C. MacKintosh, Reviews of Modern Physics **86**, 995 (2014).

[32] H. Kang, Q. Wen, P. A. Janmey, J. X. Tang, E. Conti, and F. C. MacKintosh, The Journal of Physical Chemistry B **113**, 3799 (2009).

[33] A. Kabla and L. Mahadevan, Journal of The Royal Society Interface **4**, 99 (2007).

[34] S. T. Moe, K. I. Draget, G. Skjåk-Bræk, and O. Simdsrød, Carbohydrate polymers **19**, 279 (1992).

[35] I.-L. Andresen and O. Smidsørod, Carbohydrate Research **58**, 271 (1977).

[36] C. Wang, Y. Li, and Z. Hu, Macromolecules **30**, 4727 (1997).

[37] T. Yamaue and M. Doi, The Journal of chemical physics **122**, 084703 (2005).

[38] C. Lindsey and G. Patterson, The Journal of chemical physics **73**, 3348 (1980).

[39] W. Hong, X. Zhao, J. Zhou, and Z. Suo, Journal of the Mechanics and Physics of Solids **56**, 1779 (2008).

[40] M. Doi, *Soft matter physics* (Oxford University Press, 2013).

[41] H. Nakazawa and K. Sekimoto, The Journal of chemical physics **104**, 1675 (1996).

[42] R. Lapasin, S. Paoletti, and F. Zanetti, in *Progress and Trends in Rheology II* (Springer, 1988) pp. 422–424.

[43] I. Naassaoui, O. Ronsin, and T. Baumberger, Extreme Mechanics Letters **22**, 8 (2018).

[44] Q.-M. Wang, A. C. Mohan, M. L. Oyen, and X.-H. Zhao, Acta Mechanica Sinica **30**, 20 (2014).

[45] X. Zhao, N. Huebsch, D. J. Mooney, and Z. Suo, Journal of applied physics **107**, 063509 (2010).

[46] R. N. Chacko, P. Sollich, and S. M. Fielding, Physical review letters **123**, 108001 (2019).

[47] L. Cipelletti and L. Ramos, Journal of Physics: Condensed Matter **17**, R253 (2005).

[48] O. Ronsin, C. Caroli, and T. Baumberger, Physical review letters **103**, 138302 (2009).

[49] J. Rottler and M. Warren, The European Physical Journal Special Topics **161**, 55 (2008).

[50] E. Secchi, T. Roversi, S. Buzzaccaro, L. Piazza, and R. Piazza, Soft Matter **9**, 3931 (2013).

[51] K. Kroy, Current opinion in colloid & interface science **11**, 56 (2006).

[52] A. E. Ehret, K. Bircher, A. Stracuzzi, V. Marina, M. Zündel, and E. Mazza, Nature communications **8**, 1 (2017).

Syneresis of self-crowded calcium-alginate hydrogels as a self-driven athermal aging process. — Supplementary Information—

Bruno Da Silva Pinto, Tristan Baumberger & Olivier Ronsin

1 The optical front is actually a gelation front — video

Video movie MOV.mp4 — 10 wt.% sodium alginate extruded in a 100 mM calcium chloride bath. The steel needle has a inner diameter 840 μm. In response to a slight modulation of the extrusion velocity the diameter of the fibre is not uniform (rate-controlled viscoelastic swelling). The white curves travelling from the fibre boundary towards the axis, made brighter by slightly defocussing the objective, define an optical front the diameter of which is not uniform either. A large air bubble, initially trapped into the syringe, was co-extruded with the fibre. Due to buoyancy it moves upward. Its motion and deformation clearly identifies the optical surface as a gelation front separating a solid gel shell from a liquid pregel core.

2 A minimal model for the gelation of an alginate fiber

In this section, we describe the minimal model used to analyse the kinetics of calcium induced gelation of an alginate cylinder (section 3.1.1 of the manuscript). For simplicity, we denote here the time t rather than t_1. Following Chavez et al. [1], we assume that (i) only Ca^{2+} ions diffuse from the $CaCl_2$ bath through the gelled alginate, to the gelation front of radius $r_f(t)$, and (ii) gelation there is assumed instantaneous.

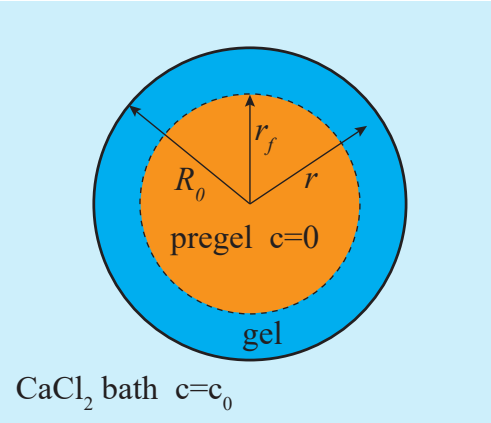

Figure 1 Cylindrical geometry of the alginate thread immersed in a $CaCl_2$ bath. Calcium ions diffuse through the shell of gelled alginate to the pregel interface where the can react to make the front advance.

In cylindrical coordinates, noting $c(r,t)$ the Ca^{2+} concentration inside the alginate gel shell and $\mathscr{D}_{\rm ion}$ the diffusion coefficient, the diffusion equation reads:

$$\frac{\partial c}{\partial t} = \frac{\mathscr{D}_{\rm ion}}{r}\frac{\partial}{\partial r}\left(r\frac{\partial c}{\partial r}\right) \tag{1}$$

with the boundary conditions (see Figure 1):

$$c(R_0,t) = c_0 \tag{2}$$

at the interface with the $CaCl_2$ bath,

$$c(r_f(t),t) = 0 \tag{3}$$

at the interface with the alginate solution, and with an initial value

$$r_f^0 = r_f(t=0) = R_0. \tag{4}$$

At the gelation front $r = r_f(t)$, per unit length of cylindrical fiber, the flux of Ca^{2+} ions $-2\pi r_f \mathscr{D}_{\rm ion}\nabla c|_{\rm r=r_f}$ provokes the gelation of a volume $-n\frac{d}{dt}(\pi r_f^2)$ of pregel, where n is the amount of ions per unit volume required to complete cross-linking. The front velocity is therefore

$$v_f = \frac{dr_f}{dt} = -\frac{\mathscr{D}_{\rm ion}}{n}\left.\frac{\partial c}{\partial r}\right|_{\rm r=r_f} \tag{5}$$

2.1 Quasi-stationary solution

When $n \ll c_0$, the front velocity is small and the concentration profile is quasi-stationary, from (1), (2) and (3):

$$c_{\rm qs}(r,t) = c_0\frac{\ln(r/r_f(t))}{\ln(R_0/r_f(t))}$$

The velocity of the gelation front is then, with (5)

$$\frac{dr_f}{dt} = -\frac{c_0\mathscr{D}_{\rm ion}}{n\ln(R_0/r_f)}\frac{1}{r_f}$$

With the initial condition $r_f(t=0) = R_0$, this integrates to

$$1 + \frac{r_f^2}{R_0^2}\left[2\ln\left(\frac{r_f}{R_0}\right) - 1\right] = \frac{4c_0\mathscr{D}_{\rm ion}t}{nR_0^2}$$

which can be rewritten in terms of the reduced front advance $\tilde{\rho}_f = 1 - r_f/R_0$:

$$\frac{1}{4} + \frac{(1-\tilde{\rho}_f)^2}{2}\left[\ln\left(1-\tilde{\rho}_f\right) - \frac{1}{2}\right] = \frac{c_0}{n}\frac{t}{\tau_{\rm ion}} \tag{6}$$

with $\tau_{\rm ion} = \dfrac{R_0^2}{\mathscr{D}_{\rm ion}}$

At short times $t \ll n\tau_{\rm ion}/c_0$, the front advance behaves as $\tilde{\rho}_f \simeq \sqrt{2t/\tau_g}$, with $\tau_{\rm ion}/\tau_g = c_0/n$ whereas complete gelation of the fiber ($\tilde{\rho}_f = 1$) occurs at time $t_g = \tau_g/4$

2.2 Numerical solution

At larger bath concentrations, the gelation front velocity is too large for the quasi-stationary solution to remain valid. The diffusion equation must be solved numerically. We used a Cranck-Nicholson scheme [2] over a regular grid of size N (chosen between 10^3 and 10^6 without significant effect on the results), spanning the gelled shell. At each time step, $dt = 2\alpha dr^2/\mathscr{D}_{\rm ion}$ with α a parameter chosen between 0.01 and 0.25 without significant effect on the results, we compute the instantaneous concentration profile. From this we extract the front velocity v_f using (5). The shell is increased accordingly. We then adapt the spatial grid step dr (keeping N constant) as well as the time step (keeping α constant). The

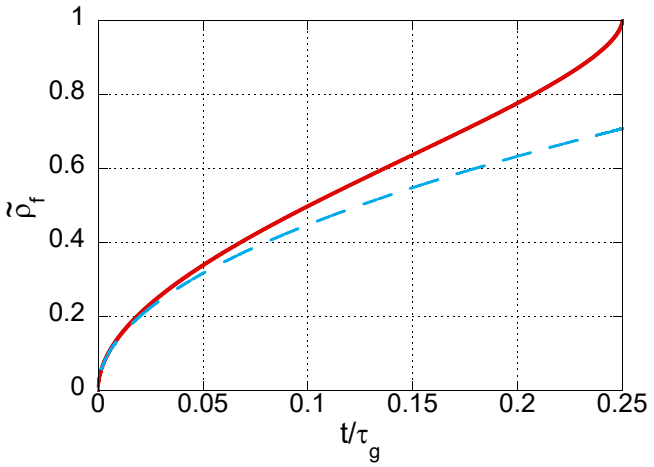

Figure 2 Full red curve : quasi-stationary evolution of the gelation front reduced position $\tilde{\rho}_f$ as a function of t/τ_g. Dotted blue curve : initial square root evolution.

concentration at new grid point is evaluated using second order polynomial interpolation.

This procedure requires a initial finite shell size d_0, with an initial concentration profile, and thus an initial value of the pregel region radius $r_f^0 = R_0 - d_0$, different from (4). However, with values of $d_0 \ll R_0$ (d_0/R_0 in the range 10^{-5}—10^{-3}), the precise concentration profile ($c(t=0,r)=0$ or $c(t=0,r)=c_{\rm qs}(r,t_0)$ with $r_f(t_0)=r_f^0$) only affects the front evolution on a time scale that remains negligible compared to $\tau_{\rm ion}$.

2.3 Results

The results presented in the following and in the manuscript where computed with $N=1000$, $\alpha=0.25$, and an initial shell thickness $d_0 = 10^{-3}R_0$ with an initial concentration profile corresponding to the quasi-stationary solution.

Figure 3 shows the evolution of the concentration profile with time for 4 different values of c_0/n, together (Fig.3.e) with the corresponding gelation front advance $\tilde{\rho}_f(t/\tau_{\rm ion})$.

We find (Figure 3.e) that the initial front advance scales as $\tilde{\rho}_f \simeq \sqrt{2t/\tau_g}$. Figure 4.a shows that $\tau_{\rm ion}/\tau_g = f(c_0/n)$ with $f(x)\simeq x$ when $x \ll 1$, recovering the quasi-stationary regime.

We can also extract the time t_g at which gelation is complete ($\tilde{\rho}_f(t_g)=1$), and the ratio t_g/τ_g is found to depend slowly with c_0/n :

$$\frac{t_g}{\tau_g} = \frac{1}{4} g\left(\frac{c_0}{n}\right)$$

with $g(x)\simeq 1$ when $x \ll 1$ as shown on Figure 4.b, recovering the quasi-stationary regime.

3 Free counterion concentration in (pre)gels

Alginate is a negatively charged polyion bearing one charge per uronate residue of average length $b = 4.8$ Å. The charge density is conveniently assessed by the parameter ξ:

$$\xi = \frac{\ell_B}{b}$$

with ℓ_B the Bjerrum length ($\ell_B = 7.1$ Å in water at 293K):

$$\ell_B = \frac{e^2}{\varepsilon k_B T}$$

with e the elementary charge, ε the bulk dielectric constant of the solvant, k_B the Boltzmann constant and T the absolute temperature.

For alginate chains at room temperature $\xi \simeq 1.5$.

A wide corpus of experimental and theoretical studies[3] indicates that, due to long ranged Coulombic interactions, as ξ exceeds a critical value ξ_c, a fraction of the counterions are no longer free to diffuse into the solvent but perform restricted motion in the immediate vicinity of the polyion. They are said to be “condensed". The simplest theoretical model, i.e. an infinite line charge with point counterions of valence z, in the limit of vanishing concentrations, yield a critical density:

$$\xi_c = \frac{1}{z}$$

This value has been found compatible with numerous experimental properties of polyelectrolyte solutions exhibiting a threshold transition controlled by the charge density ξ.

The “limiting law" theory, usually referred to as Manning condensation theory[4] predicts that for $\xi > \xi_c$, counterions condense so as to neutralize polymer charges and reduce the charge density to its critical value. The concentration of condensed counterions of valence z is therefore $C_{\rm res}\theta(z)$ with $C_{\rm res}$ the concentration of monovalent, polymer-bound charge sites and:

$$\theta(z) = \frac{1}{z}\left(1 - \frac{1}{z\xi}\right) \tag{7}$$

3.1 Sodium alginate pregels

In the sodium alginate pregel ($\xi = 1.5$, $z=1$), condition (**??**) is fulfilled at room temperature irrespective of the polymer concentration. The molar mass of sodium uronates (M of G) being 256 Da,

$$C_{\rm res} = C_A(wt.\%)\frac{10}{256}$$

This is also the total concentration of sodium ions in the solution, part of which are condensed, part of which are free to diffuse into the bulk of the pregel. In the following we will evaluate the concentrations of both counterion populations within the framework of Manning's limiting law (7). These values must be taken with a pinch of salt due to the relatively large levels of ion concentrations (with respect to the validity of limiting laws in polyelectrolytes) used in the experimental study. We assume Manning's theory to yield meaningful order of magnitudes which, for the sake of the discussion, are sufficient.

All concentrations are proportional to the alginate mass fraction C_A. Numerical values are given for a gel of concentration $C_A = 10$ wt.% for which $C_{\rm res} = 390$ mM. The concentration of condensed sodium ions is $[{\rm Na}^+]_{\rm cond} = C_{\rm res}\theta = 130$ mM. So the concentration of free sodium ions is $[{\rm Na}^+]_{\rm free} = 260$ mM.

3.2 Calcium alginate gels

In presence of calcium ions ($z=2$), the situation is more complex since part of the ions are chelated in egg-box crosslinks[5]. Note that in an egg-box dimer, chelated calcium ions neutralize half of the bound charges. Thus, the linear charge density of an egg box is the same as that of a free chain. The network is therefore homogeneously prone to counterion condensation.

Let us first assume that all sodium ions, including the condensed ones, have been permuted against calcium ions. Since $\xi > 1/2$, calcium ion condensation proceeds. With $[{\rm Ca}^{2+}]_{\rm cl}$ the concentration of chelated calcium ions, the concentration of the charge sites remaining to be neutralized is

$$c_b' = C_{\rm res} - 2[{\rm Ca}^{2+}]_{\rm cl}$$

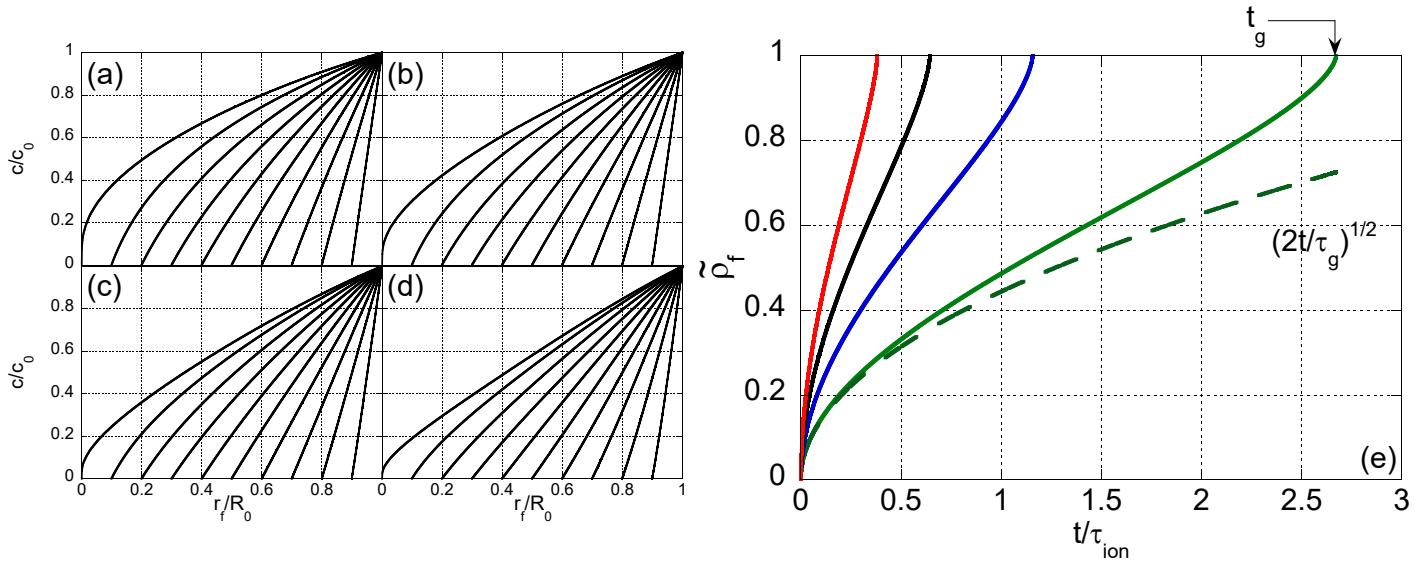

Figure 3 Evolution of the concentration profile c/c_0 as a function of r/R_0 for (a) $c_0/n = 0.1$, (b) $c_0/n = 0.25$, (c) $c_0/n = 0.5$ and (d) $c_0/n = 1$. (e) Full lines : corresponding evolution of the gelation front $\tilde{\rho}_f(t/\tau_{\rm ion})$ with increasing c_0/n from bottom to top. The dashed line is the initial square-root of time regime for the $c_0/n = 0.1$ curve.

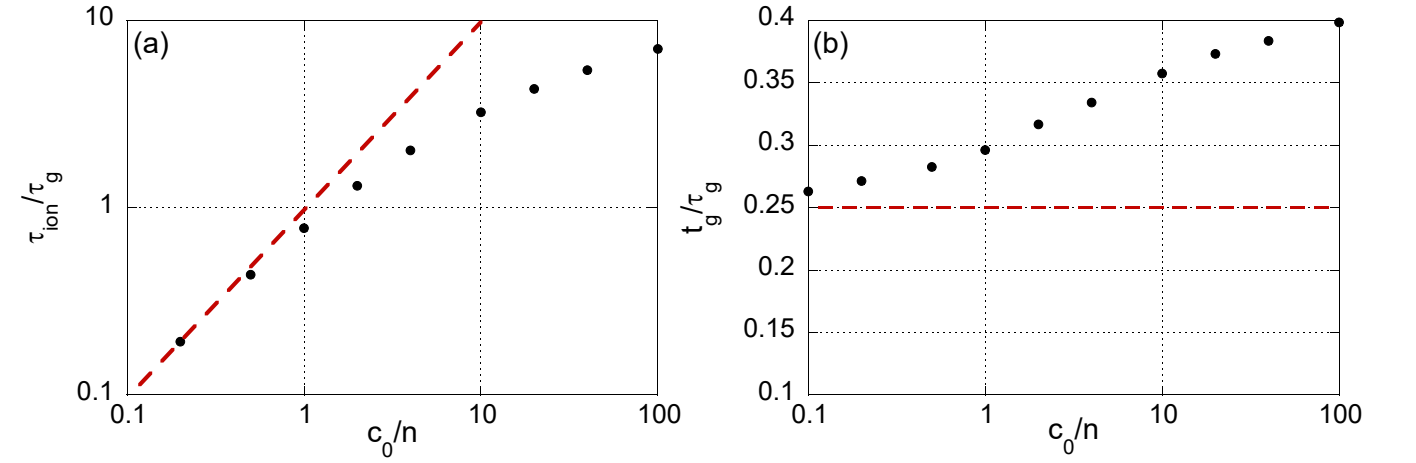

Figure 4 (a) Inverse $\tau_{\rm ion}/\tau_g$ of the characteristic time of the initial square-root advance of the gelation front as a function of the bath concentration c_0/n. (b) Ratio of the gelation time t_g and τ_g as a function of concentration c_0/n. The dashed lines are the quasi-stationary values, which are recovered, as expected, when $c_0/n \ll 1$.

The concentration of condensed calcium ions is:

$$[Ca^{2+}]_{\rm cond} = c_b' \theta(2)$$

with $\theta(2) \simeq 1/3$ since $\xi \simeq 3/2$. The total concentration of calcium ions prevented from diffusing freely in the gel is therefore:

$$[Ca^{2+}]_{\rm loc} = [Ca^{2+}]_{\rm cl} + [Ca^{2+}]_{\rm cond} = \frac{C_{\rm res} + [Ca^{2+}]_{\rm cl}}{3}$$

Assuming that both $[Ca^{2+}]$ chelation and exchange with native, condensed $[Na^+]$ are fast processes, the parameter n in the kinetic model must be identified as $[Na^+]_{\rm loc}$. A lower bound of n would be in that case $[Ca^{2+}]_{\rm loc} > C_{\rm res}/3 = 130$ mM clearly incompatible with the measured value $n \simeq 50$ mM. The calcium condensation hypothesis is therefore questionable.

The issue of *equilibrium* condensation of competing counterions of different valences has been addressed theoretically by Manning[6]. He concluded that the highest valence ions (here Ca^{2+}) condense selectively. However, in our case, some sodium counterions are already condensed in the pregel. Manning insists on the high strength of the Coulombic potential responsible for condensation. It can therefore be expected that the replacement of sodium by calcium ions, although favored by equilibrium thermodynamics, is hindered kinetically. To our knowledge this point has never be addressed, either theoretically or experimentally. In the limit of infinitely long sequestration time of condensed sodium ions, n would be attributable to the sole $[Ca^{2+}]_{\rm cl}$. Due to the chelation stoechiometry in an egg-box, $[Ca^{2+}]_{\rm cl} < C_{\rm res} FG/4$ with $FG = 0.45$ the fraction of G residues. This reads $[Ca^{2+}]_{\rm cl} < 44$ mM. The experimental $n \simeq 50$ mM pleads for densely cross-linked gels with no

calcium ion condensation.

3.3 Donnan effect

When Ca^{2+} is the sole counterion species, the global electroneutrality of the network prevents the concentration of free calcium ions inside the gel to be smaller than half the concentration of monovalent charge sites on the network which have not been neutralized by specific chelation or Manning condensation. Consequently, the concentration of calcium ions inside the gel remains larger than outside (Donnan's equilibrium[7]). Assuming that thermodynamical equilibrium has been ultimately reached so that the condensat consists exclusively of calcium ions, and that the concentration of chelated ions is $[Ca^{2+}]_{cl} = C_{res}FG/4$, the minimal amount of free ions inside the gel is:

$$c_{min} = \frac{C_{res}}{2} - C_{res}\frac{1+FG/4}{3} = 0.13\,C_{res}$$

For $C_A = 6$ wt.% (relevant to the solvent swap experiments), $C_{res} = 234$ mM and $c_{min} = 30$ mM. When $c_{swap} \gg c_{min}$, outer and inner concentrations are almost equal and osmotic pressures balance. This is the case in the initial gel prepared with $c_0 = 1$ M. When $c_{swap} \ll c_{min}$, the net osmotic pressure difference approaches $\Pi_{ion} = RTc_{min}$ with R Mayer's constant. This yields $\Pi_{ion} \simeq 80$ kPa.

Notes and references

[1] M. S. Chavez, J. A. Luna and R. L. Garrote, *Journal of food science*, 1994, **59**, 1108–1110.

[2] W. H. Press, S. A. Teukolsky, W. T. Vetterling and B. P. Flannery, *Numerical recipes 3rd edition: The art of scientific computing*, Cambridge university press, 2007.

[3] G. S. Manning, *Berichte der Bunsengesellschaft für physikalische Chemie*, 1996, **100**, 909–922.

[4] G. S. Manning, *The journal of chemical Physics*, 1969, **51**, 924–933.

[5] I. Donati, J. C. Benegas, A. Cesàro and S. Paoletti, *Biomacromolecules*, 2006, **7**, 1587–1596.

[6] G. S. Manning, *The Journal of Physical Chemistry*, 1984, **88**, 6654–6661.

[7] M. Doi, *Soft matter physics*, Oxford University Press, 2013.